Article:
Wang, J, Jin, H, Gao, H et al. (1 more author) (2022) Cooling capacity optimization of hydrocarbon fuels for regenerative cooling. Applied Thermal Engineering, 200. 117661. ISSN 1359-4311

https://doi.org/10.1016/j.applthermaleng.2021.117661

Cooling capacity optimization of hydrocarbon fuels for regenerative cooling

Jiao Wang[a], Haichuan Jin[a, *], Hui Gao[a, b], Dongsheng Wen[a, b,c, *]

[a] School of Aeronautic Science and Engineering, Beihang University, Beijing 100191, China

[b] Ningbo Institute of Technology, Beihang University, Ningbo 315800, China

[c] School of Chemical and Process Engineering, University of Leeds, Leeds LS2 9JT, U.K.

*Corresponding Authors:

Haichuan Jin

Dongsheng Wen

Email: Jinhaichuan@buaa.edu.cn;

d.wen@buaa.edu.cn

Abstract

As an effective method for heat management of hypersonic vehicles, regenerative cooling faces a severe problem of insufficient cooling capacity under high-speed conditions. Aiming to increase the cooling capacity of a given fuel, we conducted an optimization study by considering the influence of working condition, chemical kinetics and chemical routes. Via establishing a framework of multi-physical simulation by coupling the catalytic reactions with complex heat transfer process from subcritical to supercritical status, we conducted a parametric study of the effects of working conditions (i.e., inlet temperature and inlet velocity) to reveal the influence of physical heat sink, and different chemical kinetics and chemical routes to optimize the chemical heat sink. As a limiting case study, surface coking process was also investigated. With the consideration of both physical and chemical heat sinks, the regenerative cooling capacity of a hydrocarbon fuel can be effectively increased through the optimization of the working conditions. Using n-Decane as an example, a total heat sink value of 2.5 MJ/kg is obtained under typical working conditions. A maximum heat sink of 5.3 MJ/kg could be obtained by engineering chemical routes with ethylene and hydrogen as the final cracking products, under conditions 473 K and 0.042 m/s. Results also reveal that it is essential to reduce the temperature of the wall to minimize carbon deposition . For practical applications, a careful consideration of the synergies among the inlet conditions, reaction kinetics and route, and coking should be performed to optimize the cooling capacity of a HC fuel.

Keywords: Regenerative cooling; Hydrocarbon fuel; Heat-sink improvement; Thermal cracking reaction routes; Surface coking.

Nomenclature

A pre-exponential constant, s^{-1}

c concentration of products, mol/m^3

C_p constant-pressure heat capacity, $J/(kg \cdot K)$

d thickness of coking layer, m

D diameter of the regenerative cooling passages, m

D_i diffusion coefficient of i_{th} species, m^2/s

E_a activation energy in Arrhenius rate expression, kJ/mol

h enthalpy, kJ/kg

H heat sink, MJ/kg

k turbulent kinetic energy

k_A Arrhenius rate constant, $1/s$

L distance of the regenerative cooling passages, m

P_C critical pressure, MPa

p pressure, MPa

q_0 volume flow of fuel at the inlet, ml/min

R molar gas constant, 8.314 $J/(mol \cdot K)$

r radial coordinate, m

S chemical source term, $kg/(m^3 \cdot s)$

T fuel temperature, K

T_0 inlet fuel temperature, K

T_c critical temperature of i_{th} species, K

u axial velocity component, m/s

u_0 inlet axial velocity of the hydrocarbon fuel, m/s

v radial velocity component, m/s

Y_i mass fraction of i_{th} cracked product species, 1

Greeks

λ thermal conductivity, $\mathrm{W/(m \cdot K)}$

μ_i dynamic viscosity of an individual product species, $\mathrm{Pa \cdot s}$

ρ density, $\mathrm{kg \cdot m^3}$

ω_i product mass fraction of an individual product species, 1

τ viscous stress, $\mathrm{N/m^2}$

Subscripts

c coking

$chem$ chemical heat sink

$endo$ endothermic

i individual product species

in inlet of the tube

mix mixture

out exit of the tube

$prod$ products

phy physical heat sink

$reac$ reactants

tot total heat sink

w wall

1. Introduction

With the rapid development of hypersonic vehicles (HV) and increased requirement of heat management, the challenge of efficient cooling becomes more and more severe. Among various thermal protection measures, regenerative cooling, which uses the fuel to cool some critical components before it is burned in the combustor, is considered to be one of the most promising methods[1, 2]. However, as the vehicle speed increases, the demand on the cooling capacity of hydrocarbon fuels (HC fuels) also increases. It is predicted that more than 5 MJ/kg of cooling capacity[3] is required at hypersonic flow of Mach 5. The cooling capacity of a HC fuel is from two components: physical heat sink and chemical heat sink. It has been shown that when the temperature of the fuel reaches around 560 °C[4, 5], the bonds of hydrocarbon molecules become broken to produce some smaller molecules. This phenomenon, known as thermal cracking or pyrolysis, is typically endothermic and can provide further cooling capacity, called chemical heat sink, and is becoming increasingly important to meet the high cooling demand under high Mach number conditions.

Recent years see an increasing number of experimental studies on the thermal cracking characteristics and carbon deposition process of different HC fuels[6-16], aiming to increase their cooling capacity from both physical and chemical heat sink approaches. As summarized in Table 1, the maximum physical heat sink and chemical heat sink can be achieved are around 2.3 MJ/kg[15, 17, 18], and 1 MJ/kg, respectively, for pure HC fuels. As the physical heat sink is mainly decided by the initial thermophysical properties, how to enhance chemical heat sink becomes the key to further increase the cooling capacity of any HC fuels.

As shown in many prior studies[6, 19, 20], the chemical heat sink is strongly influenced by the conversion rate of the fuel and the distribution of reaction products. For instance the thermal cracking is typically endothermic if the products are unsaturated hydrocarbons (i.e., ethylene, propylene and butene) and becomes exothermic if the

products are saturated HCs such as methane[3]. Catalytic cracking is an effective way to increase the chemical heat sink of HC fuels. Properly engineered, catalytic cracking could not only increase the conversion rate, but also selectively modify the chemical routes, leading to different products. A number of catalysts have been used recently to improve chemical heat sink of different fuels[18, 21-25]. It is clearly shown in Table 1 that catalytic cracking could significantly increase the chemical heat sink. The maximum heat sink achieved so far is 4.64 MJ/kg[26] at 758 °C and 3.5 MPa by using a hybrid catalyst in zeolite matrix (Cooxides@ZSM-5). This value, however, is still less than the required cooling capacity for Mach>5, and the high temperature of >750 °C inevitably brings the problem of coking, which would significantly deteriorate the regenerative cooling performance. Clearly, how to further increase chemical heat sink while minimizing the coking phenomenon is a pressing question to answer.

Table 1 Heat sink variations of HC fuels with different kinds of catalysts.

References	HC fuels	Catalysts	Working conditions	H_{tot} (MJ/kg)	H_{phy} (MJ/kg)	H_{chem} (MJ/kg)
Jin[12]	RP-3	No catalyst	6 MPa, 699 °C	2.61	/	/
Zhu[15]	n-Decane	No catalyst	4 MPa, 670 °C	2.70	2.17	0.53
Huang[17]	JP-7	No catalyst	4.14 MPa, 635 °C	2.40	2.00	0.40
	JP-8+100	No catalyst	4.14 MPa, 734 °C	3.25	2.27	0.98
	JP-10	No catalyst	4.14 MPa, 741 °C	3.03	2.18	0.85
Yue[18]	Decalin	No catalyst	3.5 MPa ,750 °C	3.21	2.23	0.98
		Pd@N	3.5 MPa ,750 °C	3.50	2.23	1.27
Sun[27]	JP-10	No catalyst	4 MPa, 700 °C	2.32	/	/
		HDZ-O	4 MPa, 700 °C	2.80	/	/
E, X.-t.-f[28]	JP-10	No catalyst	4 MPa, 680 °C	2.09	/	/
		Pt NPs	4 MPa, 680 °C	2.71	/	/
Long[26]	n-Decane	No catalyst	3.5 MPa, 728 °C	3.77	/	/
		Cooxides@ZSM-5	3.5 MPa, 758 °C	4.64	/	/

He[22]	Methylcyclohexane	No catalyst	3.5 MPa, 690 °C	2.48	/	/
	(MCH)	PPAMAM-1	3.5MPa, 690°C	2.95	/	/
Ye[23]	Decalin	No catalyst	3.5 MPa ,675°C	2.18	/	/
		Pt @ CPAMAM	3.5 MPa ,693°C	3.03	/	/

In parallel to experimental studies, a number of numerical investigations have been conducted to examine the characteristics of thermal cracking, carbon deposition and heat transfer of HC fuels[4, 7, 8, 29-33]. Most of the simulation are based on simplified models. For a typical regenerative cooling system, the operating pressure is generally above the critical pressure of the fuel, which hence undergoes a gradually heated process in cooling channels, transiting from a sub-critical to supercritical state. The rapid change of thermophysical properties, coupling with multi-physical process of pyrolysis and trans-critical heat transfer process, makes the simulation of regenerative cooling highly challenging. How to further increase the cooling capacity of a HC fuel requires to optimize the chemical reaction route while minimizing the coking phenomenon, which is difficult to achieve experimentally.

In this work, we try to increase the cooling capacity of a given HC fuel from two approaches: i) Optimization of both working conditions and catalytic reactions, and ii) Engineering suitable reaction routes to increase the chemical heat sink while minimizing the coking effect. To achieve this, we established a framework of multi-physical simulation by coupling the catalytic reactions with complex heat transfer process from subcritical to supercritical status. We then conducted a parametric study of the effects of working conditions (i.e., inlet temperature and inlet velocity) to reveal the influence of physical heat sink, and different chemical kinetics and chemical routes to optimize the chemical heat sink. As a limiting case study, surface coking process was also investigated. As a main component of HC fuels, n-Decane has a critical pressure and temperature similar to those of actual jet fuels, and is chosen as a surrogate model to simplify the thermal cracking reactions. The result reveals the potentials of engineered low temperature catalytic cracking in maximizing the cooling capacity of a

given HC fuel.

2. Numerical methods and verifications

2.1 Physical model and boundary conditions

In order to examine the heat transfer performance and heat sink enhancement with thermal cracking, a 2D axis-symmetric model is established, as shown schematically in Figure 1. To effectively validate the simulation model, the velocity inlet and pressure outlet conditions are used for the current setting, where the experimentally measured wall temperature T_w is prescribed in the numerical study[7], as shown in Figure 2.

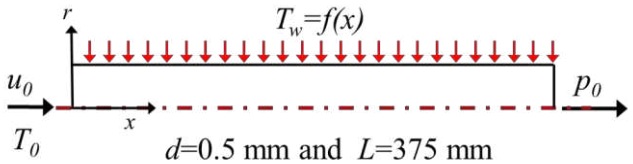

Figure 1 Schematics and boundary conditions of the simulation model.

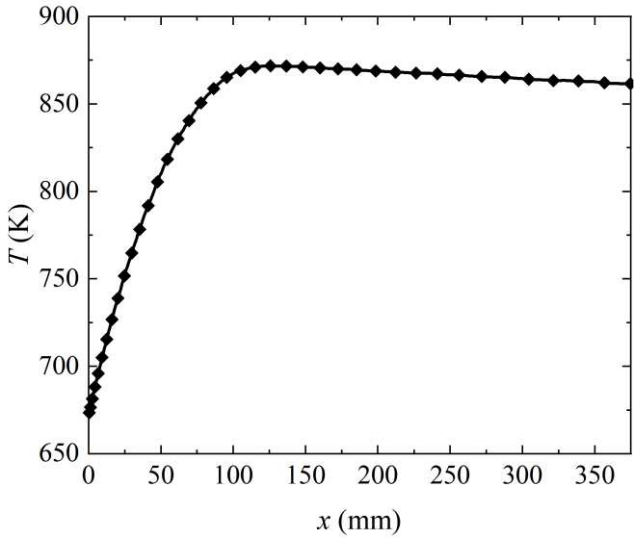

Figure 2 Thermal boundary condition: temperature distribution along the tube inner face[7]

2.2 Basic Chemical Kinetic Model

As verified in experimental results[4, 5], the initiated cracking temperature of n-

Decane is normally exceed 560 ℃. For current investigations, the baseline thermal cracking reaction kinetics of the thermal cracking of n-Decane, which consists of 18 species and one chemical reaction, is obtained from the one-step proportional product distribution (PPD) model[7] based on the experimental results.

The reaction rate of n-Decane can be defined as

$$\frac{d[C_{10}H_{22}]}{dt} = -k_A[C_{10}H_{22}] \quad (1)$$

where the rate constant, k_A, can be expressed using the Arrhenius expression:

$$k_A = Aexp\left(-\frac{E_a}{RT}\right) \quad (2)$$

More detailed information of the kinetic model and the value of pre-exponential constant A and energy activation E_a are listed in Table 2.

Table 2 PPD pyrolytic reaction kinetics model of n-Decane.

Chemical reaction	A (s^{-1})	E_a ($kJ \cdot mol^{-1}$)
$C_{10}H_{22}$→0.153CH_4+0.222C_2H_4+0.138C_2H_6+0.200 C_3H_6+0.185C_3H_8+0.171C_4H_8+0.118C_4H_{10}+0.149 C_5H_{10}+0.137C_5H_{12}+0.170C_6H_{12}+0.106C_6H_{14}+0.14 7C_7H_{14}+0.091C_7H_{16}+0.132C_8H_{16}+0.040C_8H_{18}+0.0 46C_9H_{18}+0.031C_9H_{20}	1.6×10^{15}	263.7

The PPD model has been validated in previous studies[8, 29, 31, 34] and is considered to have a high accuracy when the conversion rate of n-Decane is lower than 25%. Under higher conversion rates, as the secondary pyrolytic reactions are not taken into consideration, this model will become less accurate. However as shown by some recent work, the relative error was found to be within 15% even if the conversion reaches 70%[35], and within 20% at a conversion rate of 76%[29]. Consequently, this model can be considered to be applicable to simulate the effects of working conditions within a certain error range for flow in the whole channel.

2.3 Governing Equations and Solution Method

The governing equations for steady-state flow and heat transfer of thermal cracked n-Decane in cooling channels include mass conservation equation, momentum conservation equation, energy conservation equation, and chemical species mass fractions.

The mass conservation equation,

$$\nabla(\rho\vec{u}) = 0 \tag{3}$$

where ρ and $\vec{u}$ are the density and velocity of the fluid.

The momentum conservation equation,

$$\nabla(\rho\vec{u}\vec{u}) = -\nabla p + \nabla\tau_{eff} \tag{4}$$

where p and τ_{eff} are the pressure and viscous stress tensor.

The energy conservation equation,

$$\nabla(\rho\vec{u}e_t) = \nabla\left(\lambda_{eff}\nabla\mathrm{T}\right) - \nabla(p\vec{u}) \tag{5}$$

where e_t, λ_{eff}, and T are the total internal energy, thermal conductivity and temperature of the fluid.

The local mass fraction of each species is predicted by using a convection-diffusion equation for each component. This equation generally in the following form:

$$\nabla(\rho Y_i\vec{u}) = -\nabla(pY_iD_i) + S_i \tag{6}$$

where Y_i, D_i, S_i are the mass fraction, diffusion coefficient and chemical source term of i_{th} species.

The chemical source term S_i of equation. (6) can be solved as,

$$S_i = \dot{\omega}_\iota \cdot M_{wi} \tag{7}$$

where ω_i and M_{wi} are the chemical reaction rate and molecular weight of i_{th} species.

COMSOL Multiphysics® is used to solved the conservation equations by using four

different physics interfaces and two multiphysics coupling. As shown in Figure 3, the physics interfaces including turbulent flow, heat transfer in fluids, chemistry, and transport of concentrated species. The two multiphysics coupling interfaces include non-isothermal flow multiphysics coupling and reacting flow multiphysics coupling. Compared with conventional CFD package, COMSOL Multiphysics® make it easier to calculate chemical source terms in the species conservation equations and is more effectively in dealing with mulit-physics coupling.

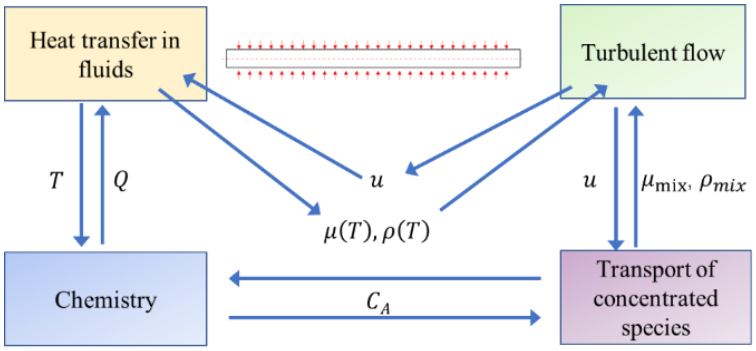

Figure 3 Coupling relationship between physical fields.

The algebraic Y+ turbulent model with Low-Re wall treatment in COMSOL Multiphysics®, which enforces a low-Reynolds-number formulation all the way down to the wall if the mesh is fine enough, is employed for accurately calculating the sharp temperature gradient and pyrolytic reactions near the wall. Therefore, the mesh near the wall needs to be fined sufficiently to allow drastically change of the fluid thermodynamic properties caused by sharp temperature gradient and pyrolytic reactions. It has been reported that the algebraic Y+ turbulent flow physics interface is suitable for incompressible flows, weakly compressible flows or compressible flows at low Mach numbers (typically less than 0.3), which is sufficient for this work.

2.4 Thermophysical properties of coolant

As introduced above, the pressure of a regenerative cooling system is normally above the critical point of the fuel to avoid the deterioration of heat transfer induced by the fuel boiling. As the temperature and pressure both reach or exceed the critical point,

the thermophysical properties of the coolant become very sensitive to the change of temperature. In this work, the SUPERTRAPP and REFPROP software developed by NIST are used to calculate the thermodynamic properties of n-Decane under a given pressure. The data is then imported into the COMSOL Multiphysics® using its user defining capability and used in subsequent calculations.

The thermodynamic properties of the mixture, such as ρ_{mix}, μ_{mix}, k_{mix}, $C_{p_{mix}}$ are determined by each component, and can be calculated as

$$\rho_{mix}(T) = \frac{1}{\Sigma_i \frac{w_i}{\rho(T)_i}} \tag{8}$$

$$\mu_{mix}(T) = \Sigma_i \frac{\mu}{1 + \sum_{j=1, j\neq i}^{n} x_j \emptyset_{ij}} \tag{9}$$

where the $\emptyset_{ij}$is given as

$$\emptyset_{ij} = \frac{(1 + (\mu(T)_i/\mu(T)_j)^{0.5}(M_i/M_j)^{0.25})^2}{(4/\sqrt{2})(1 + M_i/M_j)^{0.5}} \tag{10}$$

$$k_{mix(T)} = 0.5\left(\sum_i x_i\, k(T)_i + \sum_i (x_i\, /k(T)_i)^{-1}\right) \tag{11}$$

$$C_{p_{mix}}(T) = \Sigma_i w_i \frac{C_p(T)_i}{M_i} \tag{12}$$

3. Results and Discussion

3.1 Model validation and grid independence study

The validation of the model follows the experiments of Ward et al.[7] Detailed boundary conditions are listed in Table 3. Figure 4 presents the axial temperature, velocity, and mass fraction of n-Decane distribution in the flow direction. As shown in Figure 4, the numerical results show good agreement between the experimental and numerical data. The maximum difference between the experiments and the current

simulations are 1.9% and 9.4% for axial temperature and velocity values respectively. Consequently, the numerical model can be considered reliable and effective within a certain error range.

Table 3 Boundary conditions used for model validation.

Inlet pressure P_0 (MPa)	Temperature of the wall T_w (K)[7]	Inlet fuel temperature T_0 (K)	Inlet flow rate q_0 (ml/min)	Inlet velocity u_0 (m/s)
3.45	$f(x)$	473	0.5	0.042

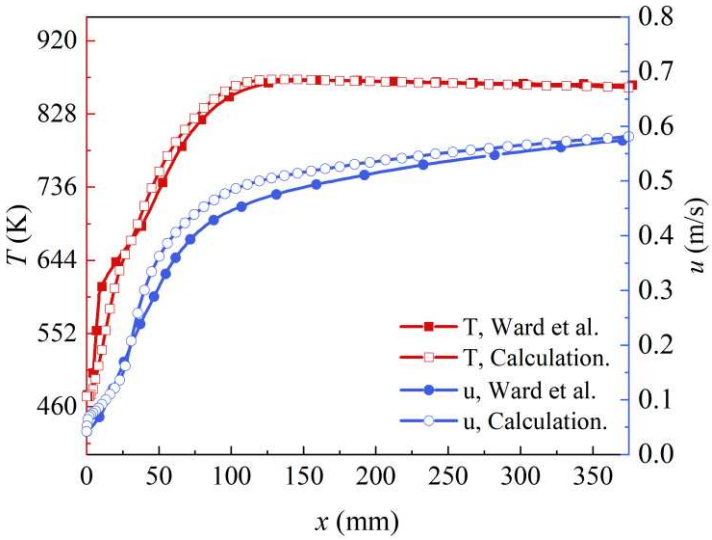

Figure 4 Distribution of axial temperature and velocity of the fuel along the tube.

Grid independence studies have been conducted before the parameterized investigations. Structured meshes are used in the axial cross section and radial cross section. Results show that a set of computational mesh of 2000 × 65 (axial × cross-sectional) are sufficient. The mesh near the wall needs to be fined due to the drastic change of the fluid thermodynamic properties caused by sharp temperature gradient and pyrolytic reactions. Totally 65 layers of meshes are used in cross-section, and 15 layers of meshes are located in the viscous layer, with the thickness of the first layer computational mesh near the wall is set to be 1 μm (i.e., satisfying the requirement of $y^+<1$). Meanwhile, the meshes near the entrance of the tube also need to be fined as the

fuel is in trans-critical state and the heat transfer process are not fully developed. The number of meshes is set to be 2000 in axial section. The growth formula is chosen as arithmetic sequence and an element ratio of 100 is used to fine the meshes near the entrance. The thickness of the first layer computational mesh near the entrance is about 4 μm.

3.2 Influence of working conditions

In this section, the PPD model is applied to study the effects of working parameters (i.e., inlet temperature and inlet velocity) on the convective heat transfer of n-Decane with endothermic thermal reactions in the range of 300-550 K and 0.001-0.1 m/s , as Table 4 shows. The parameters of chemical kinetic model remain unchanged at this state. Three cases (cases 1-3) as shown in Table 5, are used to illustrate the development of flow and temperature field, as well as the conversion rate, along the cooling channel, as shown in Figure 5 and Figure 6.

Table 4 Operating conditions for parametric studies.

Parameters	Value
Inlet pressure, P_0 (MPa)	3.45
Temperature of the wall[7],T_w (K)	$f(x)$
Inlet fuel temperature, T_0 (K)	$300-550$
Inlet velocity, u_0 (m/s)	$0.001-0.1$
Pre-exponential constant, A (1/s)	$0.8\times10^{15}-2.2\times10^{15}$
Activation energy, E_a (kJ/mol)	$230-280$
Chemical kinetic model	PPD model

Table 5 Detailed information of different cases.

Case	Inlet temperature	Inlet velocity	Pre-exponential constant	Activation energy

	T_0 (K)	u_0 (m/s)	A (1/s)	E_a (kJ/mol)
Case.1	300	0.01	1.6×10^{15}	263.7
Case.2	350	0.01	1.6×10^{15}	263.7
Case.3	300	0.02	1.6×10^{15}	263.7
Case.4	473	0.042	1.3×10^{15}	250
Case.5	473	0.042	1.5×10^{15}	250
Case.6	473	0.042	1.3×10^{15}	260

1

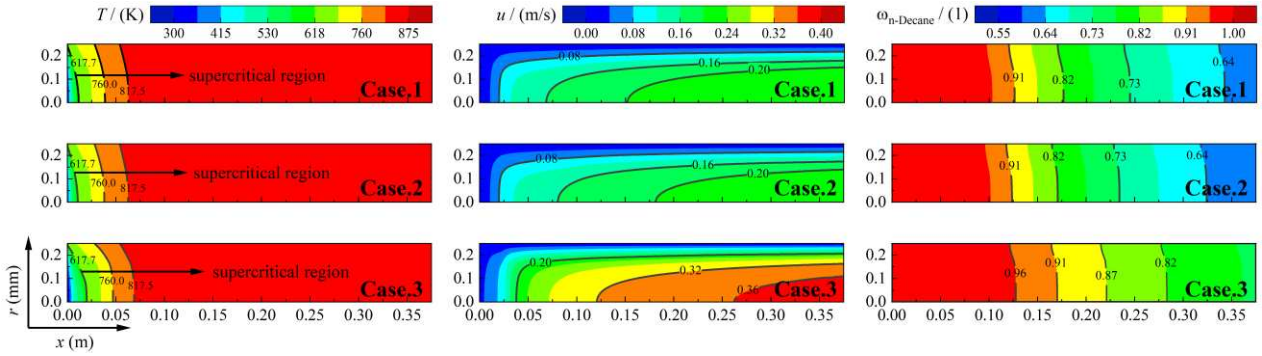

2

3 Figure 5 Distributions of fuel temperature, fuel velocity and fuel mass fraction at different inlet

4 temperatures and inlet velocities.

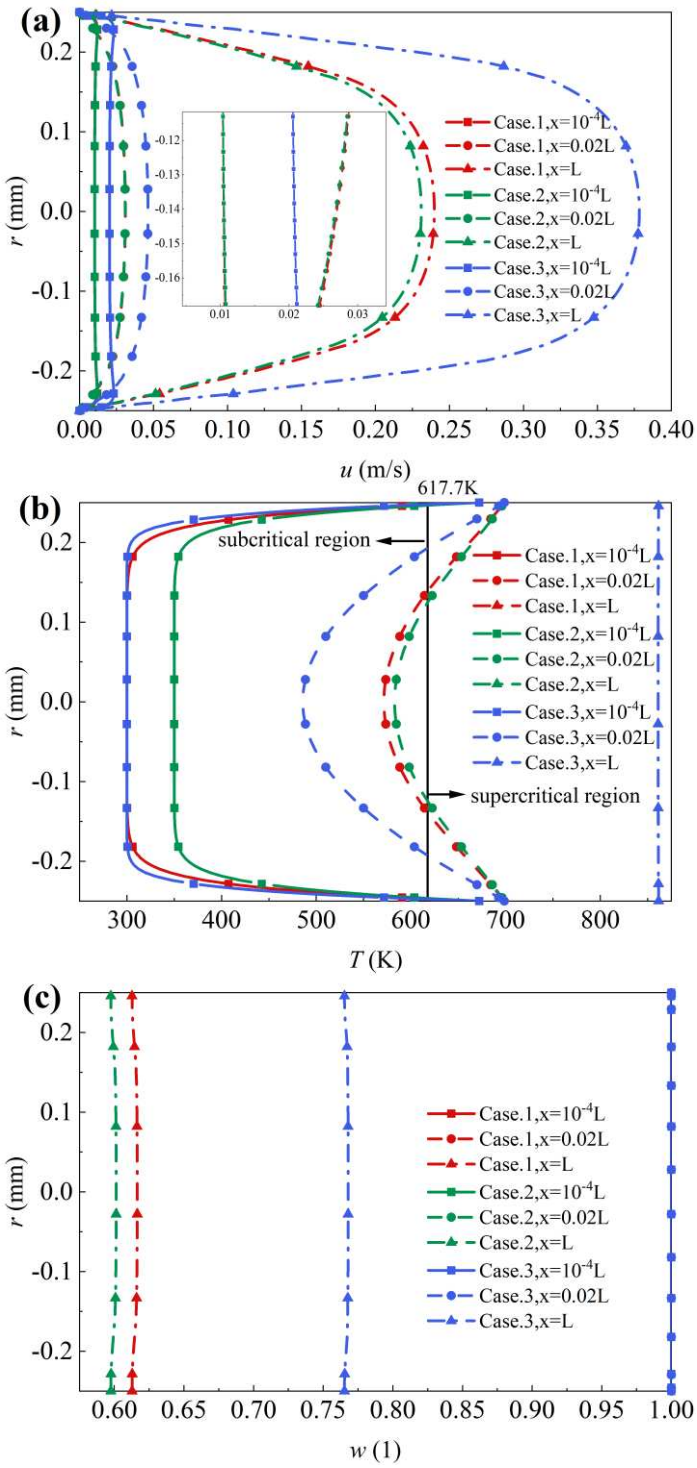

Figure 6 Variations of a) fuel velocity, b) fuel temperature and c) fuel mass fraction at different inlet temperatures and inlet velocities along radial direction at different x positions.

As mentioned before, the pressure of the tube is kept to be 3.45 MPa, which is higher than the critical pressure (2.10 MPa) of n-Decane, therefore, the fuel remains a subcritical state at the entrance. With the fluid temperature increases, the flow shall

transit into a supercritical status. However due to the rapid heating, the subcritical state occupies only a small portion in the whole cooling channel. As shown in Figure 5, regardless of the inlet temperature and velocity, the flow becomes supercritical at x/L > 5% where the temperature at the center of the channel becomes > 617.7 K, i.e., most the channel remains in the supercritical condition. The comparison between Case.1 and Case.2 indicates that as the inlet temperature is higher (i.e., Case.2), the thermal cracking starts earlier. The comparison between Case.1 and Case.3 indicates that as the inlet velocity increases, the fluid temperature reduces, which weakens the thermal cracking of n-Decane. It is clear that the variations of the inlet conditions change the flow and temperature field, leading to different conversion ratios, hence different chemical heat sinks.

Detailed variations of fuel velocity, fuel temperature and fuel mass fraction along radial direction at different x positions are shown in Figure 6. There is a quick development of the flow and temperature field within a short distance, resulting in large gradients near the wall. The conversion rate of n-Decane at the exit of the tube rises from 30.4% to 38.8% as the inlet temperature increase from 300 K (Case.1) to 350 K (Case.2). The increase of conversion rate indicates the increase of endothermic value of cracking reaction, which in turn reduces the temperature of the fuel. Moreover, the thermal cracking of n-Decane weakens as the flow velocity increases, as Figure 6 shows. At the exit of the tube, the fuel conversion rate drops from 30.4% (Case.1) to 23.5% (Case.3), which is mainly caused by the reduced temperature. As seen from Figure 6a, at the position of $x=10^{-4}$ L, the velocity near the wall is obviously higher than the axial velocity, which is caused by the sharp temperature gradient as the heat transfer process is not fully developed. The difference is mainly caused by the large variations of thermophysical properties of n-Decane as the temperature exceeds the critical point at this position. The moderate conversion ratio also supports the use of PPD model introduced in Section 2.2.

Based on the information as above, detailed heat sink distributions are calculated

using following equations

$$Q_{tot} = \sum_{i=1}^{n} \omega_{i_{out}} h(T_{out})_i - \sum_{i=1}^{n} \omega_{i_{in}} h(T_{in})_i \quad (13)$$

$$Q_{phy} = \int_1^2 C_p dT \quad (14)$$

$$Q_{chem} = Q_{tot} - Q_{phy} \quad (15)$$

A range of simulations are conducted and the heat sink distribution under different working conditions are summarized in Figure 7. With the increases of inlet temperature, the physical heat sink gradually decreases due to the reduced convective heat transfer, which can be seen from Figure 6a. However, the chemical heat sink gradually increases as the inlet temperature increases, as more fuel is thermally cracked as seen from Figure 5 and Figure 6c. As a result, the total heat sink increases as the inlet temperature decreases. Similarly, as the inlet velocity increases, the physical heat sink increases slowly but the chemical heat sink drastically drops because of the decreased temperature and reduced residence time, resulting in less fuel is thermally cracked, as shown in Figure 5, Figure 6b and Figure 6c. For comparison, at the exit of the tube, the mass fraction of n-Decane drops from 0.76 to 0.61 as the inlet velocity increases from 0.01 m/s (Case.1) to 0.02 m/s (Case.3). The density of the fuel increases as less low-molecular-weight species are formed, which causes the decreases of axial velocity, as shown in Figure 6a, Figure 6b, similar to the observation from Ref.19.

According to the heat sink map that for current regenerative cooling settings, low temperature and low inlet fuel velocity are beneficial to increase the total heat sink. The maximum physical and chemical heat sinks of 1.77 MJ/kg and 0.78 MJ/kg are obtained at 300 K and 0.1 m/s. Collectively the maximum cooling capacity within the investigated range reaches 2.51 MJ/kg at 300 K and 0.001 m/s. This value is still much smaller than the required value for hypersonic flight. There is a big scope to optimize chemical reactions to increase significantly the contribution of chemical heat sink. However, caution needs to be paid to the high temperature effect, coking might occur

that significantly reduces the performance of regenerative cooling, which is analyzed below.

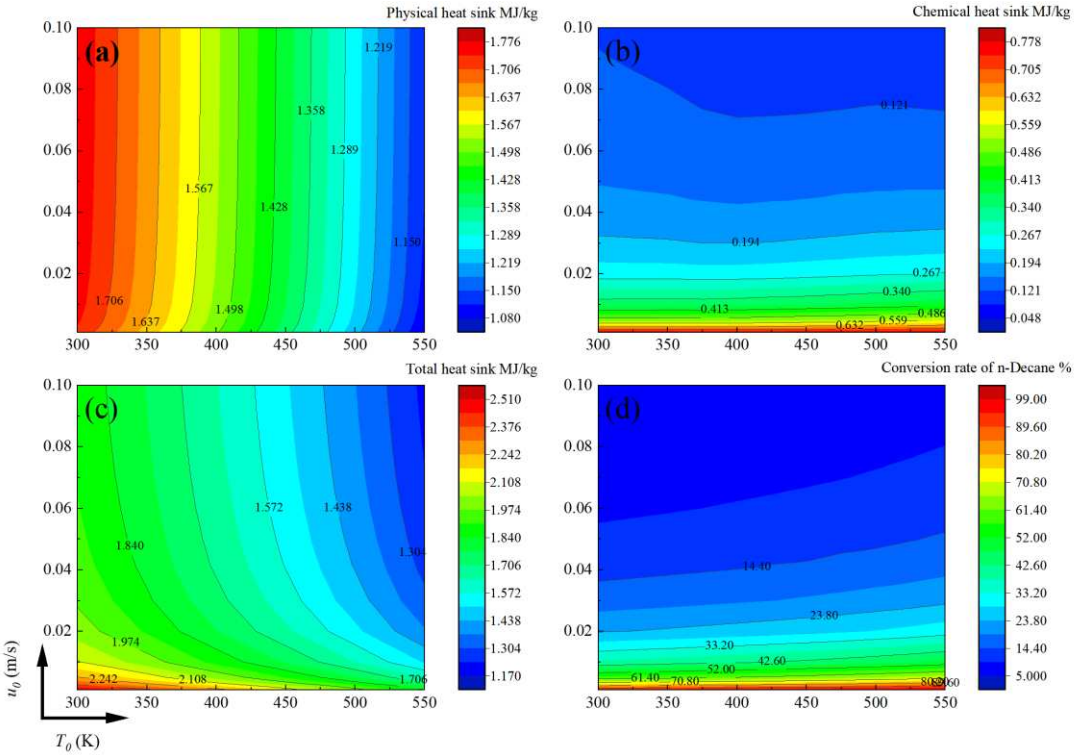

Figure 7 Distributions of a) physical heat sink, b) chemical heat sink, c) total heat sink, and d) conversion rate of n-Decane at different u_0 and T_0.

3.3 Effects of catalytic cracking models

As shown earlier, based on the optimization of working conditions, the increase of heat sink is small and the potential of chemical heat sink is not fully achieved. This section will look into the ways of maximizing chemical heat sink. The first part begins with the standard PPD model with the consideration of the effect of different catalysts by varying the values of activation energy and the pre-exponential constant. The second part looks into the possibility of different chemical reactions routes.

3.3.1 Influence of chemical kinetics (E_a/A)

The cracking process is heavily dependent on the chemical kinetics, as evidenced

by the pre-exponential constant (k) and activation energy (E_a). The choice of a catalyst is subordinated not only on the desired heat absorption level but also on the quality of the cracked products obtained for given working conditions[20]. A catalytic cracking reaction could render a very low activation energy, comparing to the thermal one[20], that promote cracking at a lower temperature. The effect of catalytic effects is represented by changing the value of A and E_a. The value of A is ranged from 0.8×10^{15} to 2.2×10^{15} 1/s and the value of E_a is ranged from 230 to 280 kJ/mol in this work. The boundary conditions are listed in Table 4. Three cases (cases 4-6) are selected from those parametric studies to illustrate the detailed variations of temperature, velocity and mass fraction of the fuel.

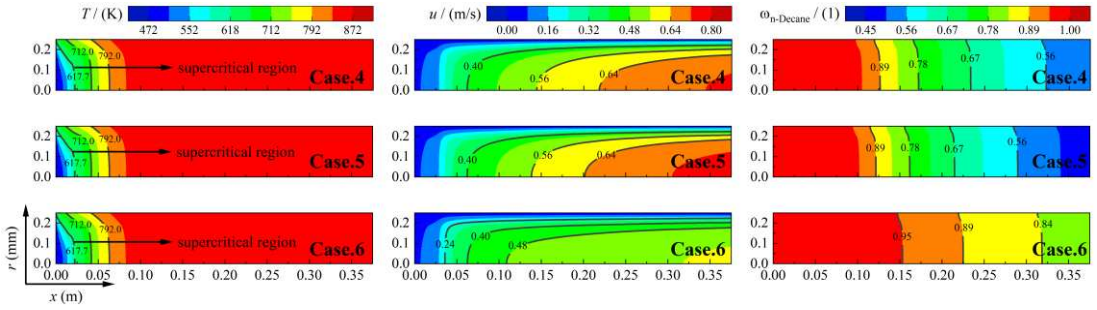

Figure 8 Variations of fuel temperature, fuel velocity and fuel mass fraction at different A and E_a.

Figure 8 show the variations of fuel temperature, fuel velocity and mass fraction of n-Decane in different cases. From the comparison of the results between Case.4 and Case.5, it is clear that the temperature of the fuel decreases when the value of A increases, which is mainly attributed to the improved conversion rate, indicating more chemical heat sink can be provided by the thermal cracking reaction. By comparing the results between Case.4 and Case.6, it shows a general trend of drastically increasing the conversion rate as the value of E_a decreases, which indicates a largely increased chemical heat sink at decreased fuel temperature. At the exit of the tube, the conversion rate increases from 49.2% to 53.2% respectively in Case.4 and Case.5, while the value drops to 19.4% in Case.6. Meanwhile, a highly cracked HC fuel produces many low-molecular-weight molecules such as ethylene, which largely decreases the density of the mixtures, leading to increased fuel velocity inside the tube.

The physical heat sink and chemical heat sink are mainly affected by the value of E_a, as shown in Figure 9a and Figure 9b. A general trend is observed that the physical heat sink decreases when the conversion rate increases, and influence of A is much smaller that of E_a. The influence of E_a to the physical heat sink is small, and the value slightly varies between 1.35-1.31 MJ/kg as the E_a reduces from 300 kJ/mol to 210 kJ/mol, due to small variations of temperature of the fluid. In contrast, the chemical heat sink increases significantly as the activation energy is reduced. For example, with a change of E_a=300 kJ/mol to 220 kJ/mol, the chemical heat sink is increased from 0.055 MJ/kg to 0.72 MJ/kg. Consequently, the chemical kinetics plays a leading role in achieving a higher cooling capacity. Within the range of parameters investigated, the maximum total heat sink of 2.09 MJ/kg for the simplified PPD model is achieved by at E_a = 220 MJ/kg. Further decreases of E_a is not encouraged as the HC has been fully converted at the exit. Such a result is very similar with those results that published in Ref.20. Different chemical reaction routes should be considered for further heat sink optimization, as described below.

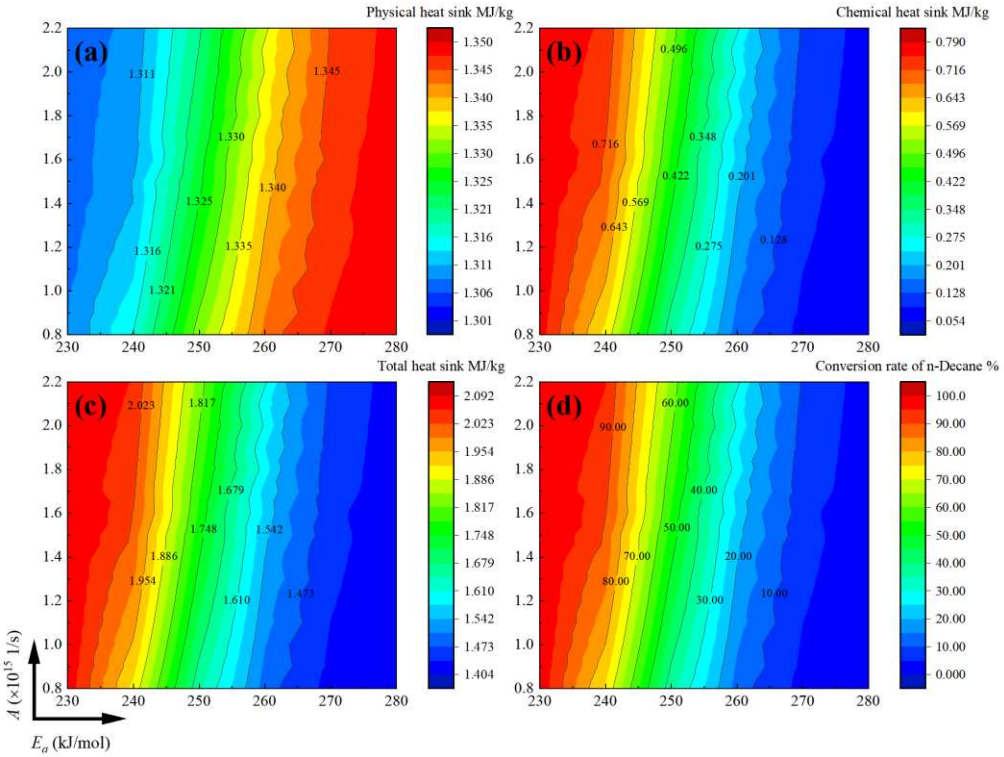

Figure 9 Distributions of a) physical heat sink, b) chemical heat sink, c) total heat sink, and d)

conversion rate of n-Decane different A and E_a.

3.3.2 Influence of different chemical routes

Some previous studies have shown that when the reaction proceeds in the direction of generating more unsaturated hydrocarbons, more cooling capacity could be obtained [36]. For example, when comparing the reaction endotherm for actual fuel cracking at high pressure to that of a notional reaction that forms 100% ethylene[19], the latter reaction could provide a cooling capacity of 3.56 MJ/kg, almost three times of the former. The PPD model above shows the influence of reaction kinetics, but could not change the chemical route as the final products are prescribed. There are many catalysts that can not only increase the reaction rate, but also cause one of several possible reactions to occur selectively. To systematically examine the effect of detailed chemical reaction routes, especially the influence of varied unsaturated hydrocarbons, another five kinds of reaction models are proposed theoretically, as shown Table 6. The theoretical chemical heat sinks at 3.45 MPa and 1000 K are calculated using the Reaction Engineering physics interface in COMSOL Multiphysics®.

Table 6 Different pyrolytic reaction kinetic model of n-Decane.

Reaction	Reaction kinetic model	Theoretical chemical heat sinks at 3.45 MPa and 1000 K (MJ/kg)
Reac.0	$C_{10}H_{22}\rightarrow 0.153CH_4+0.222C_2H_4+0.138C_2H_6+0.200C_3H_6+0.185C_3H_8+0.171C_4H_8+0.118C_4H_{10}+0.149C_5H_{10}+0.137C_5H_{12}+0.170C_6H_{12}+0.106C_6H_{14}+0.147C_7H_{14}+0.091C_7H_{16}+0.132C_8H_{16}+0.040C_8H_{18}+0.046C_9H_{18}+0.031C_9H_{20}$	0.673

Reac.1	$C_{10}H_{22}=CH_4+C_2H_4+C_3H_6+C_4H_8$	1.641
Reac.2	$C_{10}H_{22}=C_4H_8+2C_3H_6+H_2$	2.067
Reac.3	$C_{10}H_{22}=CH_4+C_3H_6+3C_2H_4$	2.361
Reac.4	$C_{10}H_{22}=2C_2H_4+2C_3H_6+H_2$	2.786
Reac.5	$C_{10}H_{22}=5C_2H_4+H_2$	3.601[19]

The chemical heat sink of different kinetic model is calculated using the following equation

$$Q_{chem} = \sum_{i=1}^{n} \omega_i h(T)_i \Big|_{prod} - \sum_{i=0}^{n} \omega_i h(T)_i \Big|_{reac} \quad (16)$$

Further investigations about the influence of different chemical kinetic models are conducted by using the same physical model in section 2.1. The boundary conditions are listed in Table 7, where the temperature of the wall is set as a constant value to simplify the computation process.

Table 7 Boundary conditions.

Inlet pressure P_0 (MPa)	Temperature of the wall T_w (K)	Inlet fuel temperature T_0 (K)	Inlet flow rate q_0 (ml/min)	Inlet velocity u_0 (m/s)
3.45	1000	473	0.5	0.042

Variations of fuel temperature and mass fraction are illustrated in Figure 10 and Figure 11, from which it can be clearly seen that with the increases of theoretical chemical heat sink, the fuel temperature decreases while the conversion rate also decreases. These results can be attributable to the increase of chemical heat absorption due to increased presence of unsaturated hydrocarbons. More detailed value of physical heat sink, chemical heat sink, total heat sink and conversion rate are shown in Figure 12.. It clears shows that different reaction routes do not change the physical heat sink saliently, but affect the chemical heat sink significantly. Among all the chemical routes

investigated, the React.5, which yield only ethene and hydrogen as the products, achieves the maximum cooling capacity of 5.312 MJ/kg, which is mainly attributable to the increase of theoretical chemical heat sink. It should be noted that the current work only investigates the theoretical possibilities of these reactions, hence different heat sinks. Whether these routes could be achieved under which catalytic conditions inside a typical regenerative cooling channel is still unclear, which clearly requires further work.

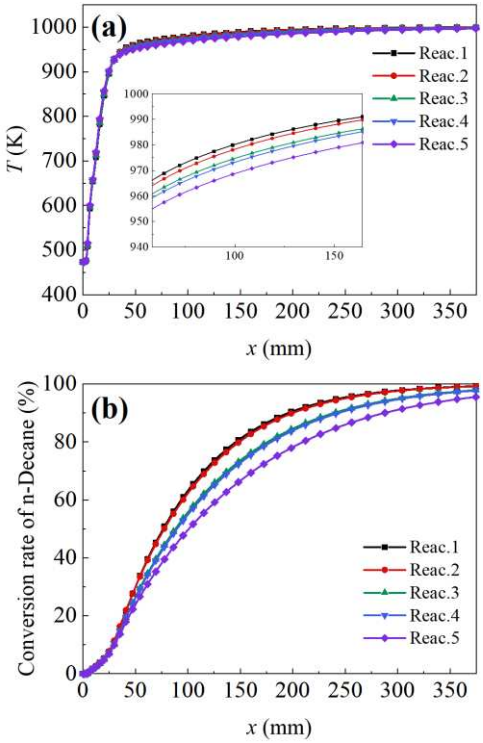

Figure 10 Distributions of a) axial temperature and b) conversion rate of n-Decane at different kinetic models.

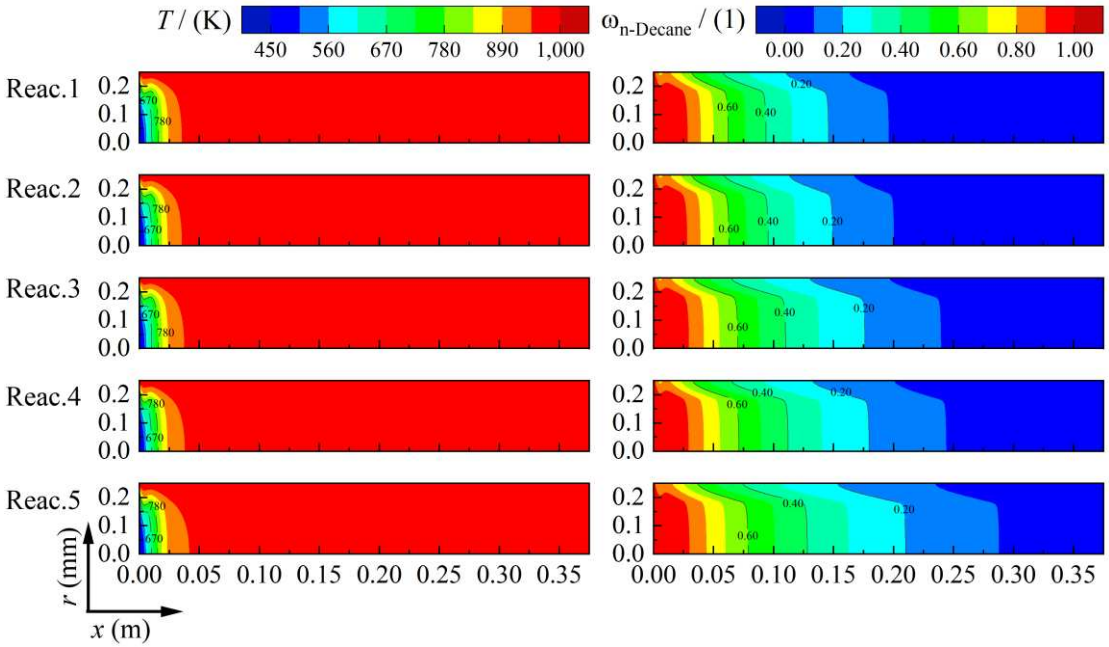

Figure 11 Variations of fuel temperature and mass fraction at different kinetic models.

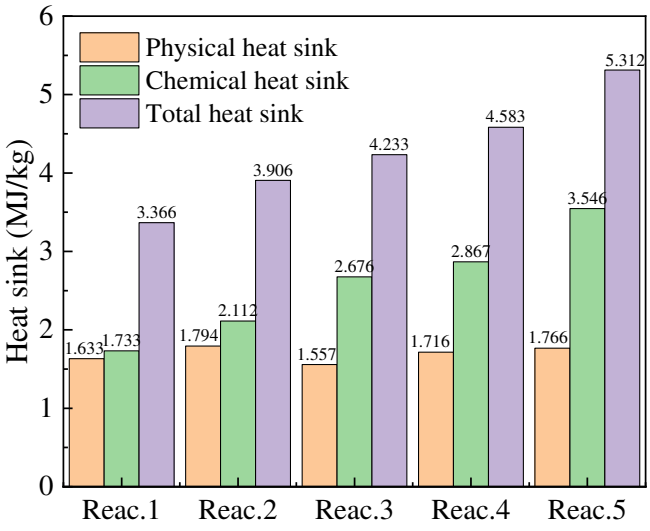

Figure 12 Heat sink distribution of different kinetic models.

3.4 Influence of surface coking under high temperature

One of the limiting conditions for any HC fuel is to avoid / minimize the carbon deposition, which needs to be carefully taken into consideration in developing regenerative cooling technology. In this part, we used a simplified model proposed Liu[9] to analyze carbon deposition on the interior surface of the cooling passages based on experimental results. In Ref.9, the MC-II model, which considered both the catalytic

coking rate and lateral coking rate is recommended to calculate the coking rate. However, as the pyrolytic kinetic model used in the research is a one-step model, the aromatics are not produced. Aromatics are regarded as the coking precursor when calculating the lateral coking rate and during the primary stage (within 20 min), meanwhile, catalytic coking rate is farther larger than lateral coking rate, hence the MC-II model no longer satisfied in this situation. Therefore, a simplified model is proposed as the model of MS-II, which regarded propene as the mainly coking precursor of n-Decane. The reliability of MS-II has been verified in previous studies[34, 37-39].

The detailed chemical kinetic parameters are listed in Table 8. These parameters were obtained by fitting the experimental data of the overall mass of carbon deposition.

Table 8 Chemical kinetic parameters of MS-II model.

	k_{c0}	E_{a1}	n	γ
	$\mu g \cdot cm^2 \cdot min^{-1}/(mol \cdot L)^{-1}$	kJ/mol	1	1
MS-II	8.68×10^{11}	192.88	0.46	0.074

As introduced before, propene is the key coking precursor. As the thickness of the deposited carbon is very thin within the relatively short period, its effects on fluid dynamics and heat transfer can thus be safely neglected. Therefore, the steady-state numerical results, including the surface temperature and molar concentration of propene at the tube wall, are directly used to study surface coking.

$$\frac{dSC}{dt}(\mathrm{t}) = k_{c0} e^{-E_{a1}/RT_w(z)} e^{-\mathrm{t}\gamma} C(C_3H_6)^n \quad (17)$$

The density of coke is 1883 kg/m^3 according to the measurement of Gascoin et al.[40]. As the equation indicates, a higher propene concentration can lead to more surface carbon deposition. For a set wall temperature, the coking rate is only affected by the molar concentration of propene. As n-Decane is progressively cracked, the coking precursor of propene is produced, as shown in Figure 13a. Under the condition of Reac.3 and Reac.5, shown in Figure 13b, the amount of carbon deposition on the inner surface of the tube are relatively small when compared with other conditions. The

maximum thickness of carbon deposition occurred at the condition of Reac.2 at the exit of the tube, with the value of 1.32×10^{-3} mm, which is around 0.528% of the radius of the tube.

Besides the effect of concentration of propene, the effect of wall temperature on the thickness of the carbon deposition layer within 0-10 min is also studied by using the maximum value of concentration of propene in different reaction routes. The value is 95.438 mol/m^3, 188.42 mol/m^3, 77.117 mol/m^3, 152.24 mol/m^3, and 0 mol/m^3, respectively for Reac.1, Reac.2, Reac.3, Reac.4 and Reac.5. Detailed distributions are shown in Figure 13c, where it shows that with increasing temperature, the thickness of the carbon deposition layer increase only slightly at the beginning. However, as the temperature exceeds around 1050 K, the coking rate increases significantly, which would clearly deteriorate the cooling performance. As there is still no definition of a critical coking thickness that should not be exceeded, we will define a critical deposition thickness as 5% of the inner radius value, corresponding to 0.0125 mm in this work. It is clearly seen from Figure 13c that in order to satisfy the maximum limitation of thickness of the carbon deposition layer, the temperature of the wall need to kept below a certain value, which is around 1121 K, 1106 K, 1127 K, 1111 K, respectively for Reac.1, Reac.2, Reac.3, Reac.4. The maximum difference is 21 K and it is a wider temperature range for Reac. 3 to satisfy this limitation. This result indicates that, to effectively reduce the thickness of the carbon deposition caused by thermal cracking of n-Decane, it is more important to reduce the temperature of the wall, which further illustrates the importance of the optimum of cooling capacity for HC fuels. However, it should be noted that as ethylene is not regarded as the carbon precursor of n-Decane in these cases, as shown no carbon deposition for Reac.5. whose effects need to further investigated.

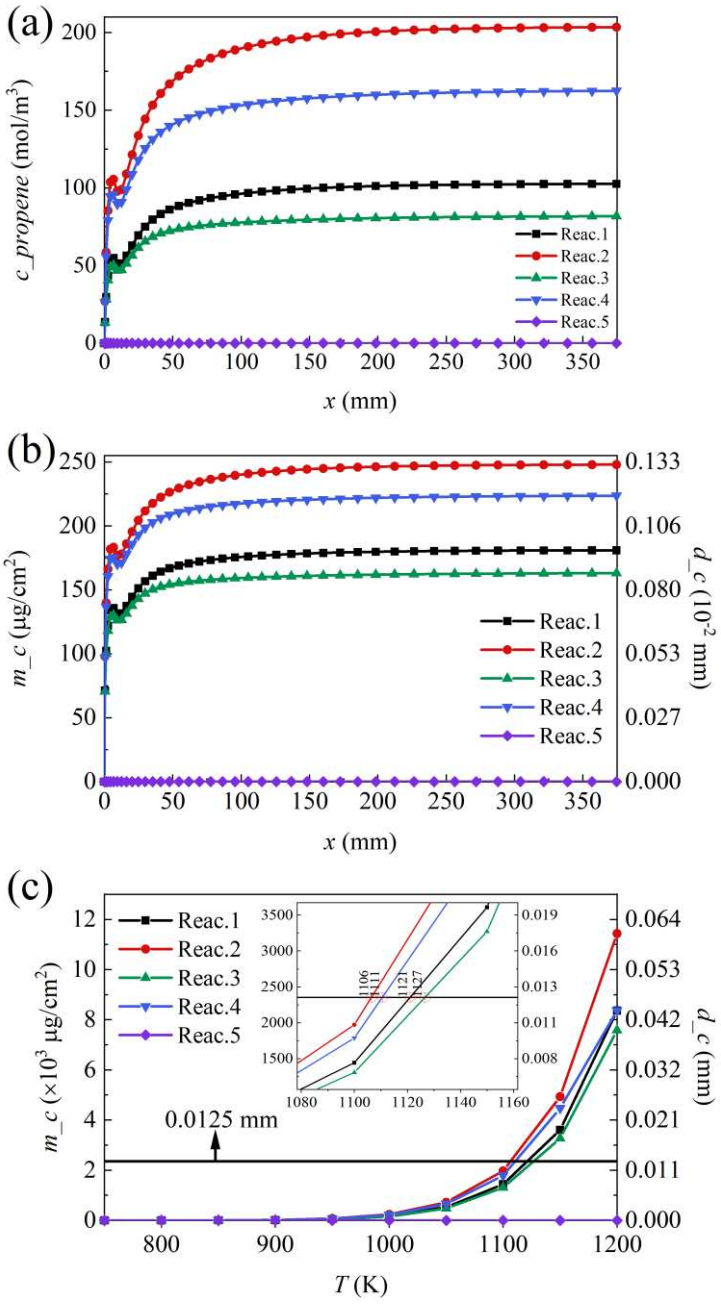

Figure 13 Distributions of (a) propene concentration (b) amount of surface carbon deposition within 0-10 min (c) thickness of surface carbon deposition within 0-10 min and (d) change of coking rate with temperature 0-10 min

4. Conclusion

In this work, a series of numerical studies are conducted to optimize the working

condition and reaction route as to maximize the cooling capacity of hydrocarbon fuels. A parametric study of the effects of basic fluid parameters (i.e., inlet temperature and inlet velocity), chemical kinetic model parameters and different chemical kinetic models on the flow and heat transfer of n-Decane is conducted. The reliability of model is validated by comparing with published experimental data, including fuel temperature and velocity, and the main conclusions can be summarized as

- According to the heat sink map that for current regenerative cooling settings, low inlet temperature and inlet velocity are beneficial to increase the total heat sink. The maximum cooling capacity of 2.509 MJ/kg is achieved at 300 K and 0.001 m/s for n-decane.
- A general trend shows that a higher pre-exponential constant and a lower activation energy is conductive to the cracking reaction. The maximum total heat sink of 2.09 MJ/kg is achieved by reducing the value of E_a to 220 kJ/mol. The heat sink distribution show less correlation with the value of A than that of E_a.
- Five types of chemical kinetic model are used to study the influence of unsaturated hydrocarbons. The larger the proportion of unsaturated hydrocarbons in the product, the more beneficial for increasing the chemical heat sink. The maximum cooling capacity of 5.3 MJ/kg is achieved when the products are ethylene and hydrogen only.
- The phenomena of surface carbon deposition are analyzed on the basis of simplified MS-II pyrolytic surface coking model. The maximum thickness of carbon deposition occurred at the condition of Reac.2 at the exit of the tube, with the value of 1.32×10^{-3} mm, ~ 0.528% of the radius of the tube.
- For practical applications, a careful consideration of the synergy among the inlet conditions, reaction kinetics and route, and coking should be performed to optimize the cooling capacity of a HC fuel.

References

1. Jackson, T. A.; Eklund, D. R.; Fink, A. J., High speed propulsion: Performance advantage of advanced materials. *J Mater Sci* **2004,** *39* (19), 5905-5913.
2. Edwards, T., Liquid fuels and propellants for aerospace propulsion: 1903-2003. *Journal of Propulsion and Power* **2003,** *19* (6), 1089-1107.
3. Lander, H.; Nixon, A. C., Endothermic Fuels for Hypersonic Vehicles. *Journal of Aircraft* **1971,** *8* (4), 200-207.
4. Zhao, G.; Song, W.; Zhang, R., Effect of pressure on thermal cracking of china RP-3 aviation kerosene under supercritical conditions. *International Journal of Heat and Mass Transfer* **2015,** *84*, 625-632.
5. Jiang, Y.; Qin, J.; Chetehouna, K.; Gascoin, N.; Bao, W., Effect of geometry parameters on the hydrocarbon fuel flow rate distribution in pyrolysis zone of SCRamjet cooling channels. *International Journal of Heat and Mass Transfer* **2019,** *141*, 1114-1130.
6. Stewart, J.; Brezinsky, K.; Glassman, I., Supercritical Pyrolysis of Decalin, Tetralin,and N-Decane at 700—800K. Product Distribution and Reaction Mechanism. *Combustion Science and Technology* **1998,** *136* (1), 373-390.
7. Ward, T. A.; Ervin, J. S.; Striebich, R. C.; Zabarnick, S., Simulations of Flowing Mildly-Cracked Normal Alkanes Incorporating Proportional Product Distributions. *Journal of Propulsion and Power* **2004,** *20* (3), 394-402.
8. Ward, T. A.; Ervin, J. S.; Zabarnick, S.; Shafer, L., Pressure Effects on Flowing Mildly-Cracked n-Decane. *Journal of Propulsion and Power* **2005,** *21* (2), 344-355.
9. Liu, G.; Wang, X.; Zhang, X., Pyrolytic depositions of hydrocarbon aviation fuels in regenerative cooling channels. *Journal of Analytical and Applied Pyrolysis* **2013,** *104*, 384-395.
10. Jiang, R.; Liu, G.; He, X.; Yang, C.; Wang, L.; Zhang, X.; Mi, Z., Supercritical thermal decompositions of normal- and iso-dodecane in tubular reactor. *Journal of Analytical and Applied Pyrolysis* **2011,** *92* (2), 292-306.
11. Zhong, F.; Fan, X.; Yu, G.; Li, J., Thermal cracking of aviation kerosene for scramjet applications. *Science in China Series E: Technological Sciences* **2009,** *52* (9), 2644-2652.
12. Jin, B.; Jing, K.; Liu, J.; Zhang, X.; Liu, G., Pyrolysis and coking of endothermic hydrocarbon fuel in regenerative cooling channel under different pressures. *Journal of Analytical and Applied Pyrolysis* **2017,** *125*, 117-126.
13. Li, Z.; Wang, H.; Jing, K.; Wang, L.; Li, Y.; Zhang, X.; Liu, G., Kinetics and modeling of supercritical pyrolysis of endothermic hydrocarbon fuels in regenerative cooling channels. *Chemical Engineering Science* **2019,** *207*, 202-214.
14. Li, Z.; Liu, G.; Zhang, R., Heat transfer to supercritical hydrocarbon fuel in horizontal tube: Effects of near-wall pyrolysis at high heat flux. *Chemical*

Engineering Science **2021,** *229*.
15. Zhu, Y.; Liu, B.; Jiang, P., Experimental and Numerical Investigations onn-Decane Thermal Cracking at Supercritical Pressures in a Vertical Tube. *Energy & Fuels* **2013,** *28* (1), 466-474.
16. Zhang, S.; Feng, Y.; Jiang, Y.; Qin, J.; Bao, W.; Han, J.; Haidn, O. J., Thermal behavior in the cracking reaction zone of scramjet cooling channels at different channel aspect ratios. *Acta Astronautica* **2016,** *127*, 41-56.
17. Huang, H.; Spadaccini, L.; Sobel, D., Endothermic Heat-Sink of Jet Fuels for Scramjet Cooling. In *38th AIAA/ASME/SAE/ASEE Joint Propulsion Conference & Exhibit*, 2002.
18. Yue, L.; Lu, X.; Chi, H.; Guo, Y.; Xu, L.; Fang, W.; Li, Y.; Hu, S., Heat-sink enhancement of decalin and aviation kerosene prepared as nanofluids with palladium nanoparticles. *Fuel* **2014,** *121*, 149-156.
19. Edwards, T., Cracking and Deposition Behavior of Supercritical Hydrocarbon Aviation Fuels. *Combustion Science and Technology* **2006,** *178* (1-3), 307-334.
20. Heinrich, B.; Luc-Bouhali, A.; Ser, F.; Vigot, C., Endothermic liquid fuels - Some chemical considerations on the cooling process. In *10th AIAA/NAL-NASDA-ISAS International Space Planes and Hypersonic Systems and Technologies Conference*, 2001.
21. Huang, B.; Shrestha, U.; Davis, R. J.; Chelliah, H. K., Endothermic Pyrolysis of JP-10 with and without Zeolite Catalyst for Hypersonic Applications. *AIAA J* **2018,** *56* (4), 1616-1626.
22. He, G. J.; Wu, X.; Ye, D. F.; Guo, Y. S.; Hu, S. L.; Li, Y.; Fang, W. J., Hyperbranched Poly(amidoamine) as an Efficient Macroinitiator for Thermal Cracking and Heat-Sink Enhancement of Hydrocarbon Fuels. *Energy & Fuels* **2017,** *31* (7), 6848-6855.
23. Ye, D. F.; Zhao, L.; Bai, S. S.; Guo, Y. S.; Fang, W. J., New Strategy for High-Performance Integrated Catalysts for Cracking Hydrocarbon Fuels. *Acs Appl Mater Inter* **2019,** *11* (43), 40078-40090.
24. Yue, L.; Wu, J.; Gong, Y.; Fang, W., Thermodynamic properties and pyrolysis performances of hydrocarbon-fuel-based nanofluids containing palladium nanoparticles. *Journal of Analytical and Applied Pyrolysis* **2016,** *120*, 347-355.
25. Kim, S.; Sasmaz, E.; Pogaku, R.; Lauterbach, J., Effects of reaction conditions and organic sulfur compounds on coke formation and HZSM-5 catalyst performance during jet propellant fuel (JP-8) cracking. *Fuel* **2020,** *259*.
26. Long, L.; Lan, Z. Z.; Han, Z. X.; Qiu, Y. F.; Zhou, W. X., Co3O4 Nanosheet Wrapped Commercial HZSM-5 for Promoting Catalytic Cracking of n-Decane and Anticoking Activities. *ACS Appl Energ Mater* **2018,** *1* (8), 4130-4139.
27. Sun, W.; Liu, G.; Wang, L.; Zhang, X., Quasi-homogeneous catalytic cracking of JP-10 over high hydrocarbon dispersible nanozeolites. *Fuel* **2015,** *144*, 96-102.

28. E, X.-t.-f.; Zhang, Y.; Zou, J.-J.; Wang, L.; Zhang, X., Oleylamine-Protected Metal (Pt, Pd) Nanoparticles for Pseudohomogeneous Catalytic Cracking of JP-10 Jet Fuel. *Industrial & Engineering Chemistry Research* **2014,** *53* (31), 12312-12318.
29. Bao, W.; Zhang, S. L.; Qin, J.; Zhou, W. X.; Xie, K. L., Numerical analysis of flowing cracked hydrocarbon fuel inside cooling channels in view of thermal management. *Energy* **2014,** *67*, 149-161.
30. Feng, Y.; Qin, J.; Bao, W.; Yang, Q.; Huang, H.; Wang, Z., Numerical analysis of convective heat transfer characteristics of supercritical hydrocarbon fuel in cooling panel with local flow blockage structure. *The Journal of Supercritical Fluids* **2014,** *88*, 8-16.
31. Ruan, B.; Meng, H.; Yang, V., Simplification of pyrolytic reaction mechanism and turbulent heat transfer of n-decane at supercritical pressures. *International Journal of Heat and Mass Transfer* **2014,** *69*, 455-463.
32. Xu, K.; Meng, H., Model validation and parametric study of fluid flows and heat transfer of aviation kerosene with endothermic pyrolysis at supercritical pressure. *Propulsion and Power Research* **2015,** *4* (4), 202-211.
33. Xu, K.; Meng, H., Modeling and Simulation of Supercritical-Pressure Turbulent Heat Transfer of Aviation Kerosene with Detailed Pyrolytic Chemical Reactions. *Energy & Fuels* **2015,** *29* (7), 4137-4149.
34. Tao, Z.; Hu, X.; Zhu, J.; Cheng, Z., Numerical Study of Flow and Heat Transfer ofn-Decane with Pyrolysis and Pyrolytic Coking under Supercritical Pressures. *Energy & Fuels* **2017,** *31* (8), 8698-8707.
35. Feng, Y.; Zhang, S. L.; Cao, J.; Qin, J.; Cao, Y.; Huang, H. Y., Coupling relationship analysis between flow and pyrolysis reaction of endothermic hydrocarbon fuel in view of characteristic time correlation in mini-channel. *Appl Therm Eng* **2016,** *102*, 661-671.
36. Feng, Y.; Qin, J.; Liu, S.; Zhang, S.; Li, X.; Cao, Y.; Huang, H., A simplification of pyrolytic reaction model of hydrocarbon fuel and its application in simulation of heated channel flow. *International Journal of Thermal Sciences* **2018,** *130*, 10-18.
37. Xu, K.; Meng, H., Numerical study of fluid flows and heat transfer of aviation kerosene with consideration of fuel pyrolysis and surface coking at supercritical pressures. *International Journal of Heat and Mass Transfer* **2016,** *95*, 806-814.
38. Sun, X.; Xu, K. K.; Meng, H., Supercritical-Pressure Heat Transfer, Pyrolytic Reactions, and Surface Coking of n-Decane in Helical Tubes. *Energy & Fuels* **2018,** *32* (12), 12298-12307.
39. Pan, Y.; Zhang, H.; Zhang, C.; Wang, H.; Jing, K.; Wang, L.; Zhang, X.; Liu, G., Supercritical Pyrolysis and Coking of JP-10 in Regenerative Cooling Channels. *Energy & Fuels* **2020,** *34* (2), 1627-1638.
40. Gascoin, N.; Gillard, P.; Bernard, S.; Bouchez, M., Characterisation of

coking activity during supercritical hydrocarbon pyrolysis. *Fuel Processing Technology* **2008,** *89* (12), 1416-1428.

Acknowledgements

This work was supported by the National Natural Science Foundation of China (No. 51906010) and the National Numerical Wind tunnel (Grant 2018-ZT3A05).